High Efficiency Triple-Junction Solar Cell for Portable Device Charging Applications

Karen Yang
Department of Electrical Engineering
University of Illinois at Urbana-Champaign, Urbana, IL 61801, USA

Abstract

Traditionally, high efficiency solar cells based on III-V materials have been limited to space-exploration applications due to their high cost. With the technological maturity of silicon-based solar panels, however, using these III-V cells in terrestrial applications is a possible next step towards widespread solar adoption. Specifically with high reliance of the current generation of children and adults on portable electronic devices such as iPads for entertainment and iPhones for GPS navigation, integrating solar energy into these devices would remove parental stress related to bringing five different charging cables to charge devices and the potential to be stranded without GPS guidance. Thus, proposed here is the design for an iPad case containing an array of triple-junction solar cells to provide direct power to the device while it is on and storage of electricity in an attachable battery when the device is powered off. The surface area available for solar panels on an iPad is extremely limited and is not enough for a solar array based on commercial silicon panels to power the device, as the panels only have an efficiency of around 20%. [1] With a triple-junction solar cell design based on III-V materials, however, array efficiencies have been shown to exceed 40%, reducing the amount of space needed by a factor of two. [2] While the solar array will not be able to instantaneously supply the power needed to constantly charge the device, the cell simulated here with CrossLight TCAD software was designed such that the operational condition is at the maximum power point while matching the output current and voltage to that of a lithium-ion battery. The layer thicknesses and doping levels were adjusted to satisfy the criteria previously mentioned. Simulations were done for the standard AM1.5 solar spectrum, and a brief financial feasibility analysis was conducted to determine how much expense the attached solar array would add to the price of an iPad case. The electrical simulation results and financial feasibility calculations are detailed in the body of this paper.

I. Introduction/Motivation

While terrestrial solar cell technology based on silicon and extraterrestrial solar cells based on III-V materials have reached a certain level of technological maturity, there has yet to be a major push towards applying these high efficiency cells traditionally made for space exploration to terrestrial applications. Further, although this may be a niche market for those able to afford devices which integrate expensive but highly efficient multijunction III-V cells into everyday electronics, the market for high end electronics is certainly undergoing rapid growth, especially with wealthy influencers and the Gen Z generation. Thus, the goal of this project is to develop a solar cell stack optimized for the integration into handheld electronics such as iPads and iPhones.

A major challenge in the widespread integration of solar cells into everyday objects is the amount of space and weight a panel adds to the device. The use of multi-junction III-V solar cells with luxury electronics would help mitigate these concerns while providing a source of instant electricity not reliant on batteries or charging cables, both of which add bulk and are easily forgotten. The addition of a non-depletable source of energy to electronic devices would be especially beneficial in emergency situations. For example, it would allow a lost hiker to continuously attempt to contact emergency response services without fear of their phone battery depleting. Even in less dire situations, it would prevent a tourist from being lost in an unfamiliar city, as the attached solar array could charge the device to provide GPS navigation, or even prevent a meltdown by a toddler when his iPad runs out of charge. From an environmental standpoint, although charging electronic devices does not constitute a large portion of

residential or commercial electricity usage, applying the same design process outlined here to applications such as streetlights and stoplights would greatly reduce a city's reliance on non-renewable energy resources such as natural gas and coal.

There are currently three approaches to integrating PV with mobile devices: transparent solar cells within the screen of the phone, an opaque solar cell mounted on the back of the device with either thin film or silicon materials, and an external solar panel that charges the phone via a cord.

The transparent solar cell option clearly has the lowest profile and is adaptable to the greatest number of devices, but the current efficiency of fully transparent solar cells is around 2%. [3] It would also need to be compatible with any sensors such as fingerprint scanners imbedded into the smartphone screen, which may further reduce its efficiency. While this may be enough to trickle charge the phone, if the phone is completely dead, it will likely not be able to supply enough power to start up the phone. With an external solar module charging the phone via a cable, this certainly would provide more electricity, as the transparency of the cell is not a constraint. Although it would still need to be small and portable, an external array would not be strictly constrained to the size of the device. However, this is still an external module which will need to be packed alongside any cables.

Currently, the most technologically realistic option is to mount a solar array on the back of the phone or directly under the glass. This may take the form of a flexible thin film module which would add virtually no weight to the phone or case, or the high efficiency module designed here. Putting it under the glass would allow for the most amount of sunlight to be absorbed, as most phone usage is with the screen facing the sun, but the entire screen would have to be redesigned to be able to contact the processor and other chips in the device through the solar cell. This is huge technological hurdle and would require complete upheaval of existing smartphone designs. Although mounting a panel on the back of a case would naturally receive less sunlight since hands will block much of the panels, this option presents the smallest leap in technology, since it is simply a matter of adding an existing panel to a case which can charge the phone via wireless charging. One solar cell material which may be a promising candidate is CdTe thin film cells, as they add virtually no weight and can easily be applied to a case. However, the efficiency of thin film cells such as CdTe is around 18%. [4] While that is certainly a huge boost up from the 2% efficient transparent cells, this may not be enough to power and charge the device, especially as processing intensity increases.

Thus, the design in this report will focus on using expensive but highly efficient multijunction solar cells based on III-V materials. Especially considering the limited amount of irradiance reaching the back of a phone under typical usage, the efficiency is a crucial factor in the success of a solar powered cell phone. Further, leaving the device upside down in the sun for long periods of time to charge it would lead to the device heating up, potentially damaging internal processes. This is another reason why III-V cells would be a better solution over lower efficiency options, which would take longer to charge. Considering the technological maturity of III-V cells combined with unique design considerations required of mobile device usage, integrating a III-V array to the back of a cell phone or tablet is the most realistic option of powering mobile devices with solar power in the near term.

Three cell geometries were simulated and evaluated based on the power conversion efficiency and financial feasibility of each option. The traditional InGaP/GaAs/Ge monolithic triple-junction solar cell was evaluated as the first option. While this structure is the most common triple junction structure, its demonstrated efficiency is about 32.3%. [5] An alternative InGaP/GaAs/InGaAs inverted metamorphic (IMM) structure with a graded buffer region was also simulated, as the demonstrated efficiency is around 33.8%. [6] However, the structure that was ultimately optimized and proposed here is a four terminal cell consisting of a dual junction InGaP/GaAs cell mechanically stacked on a single junction InGaAs cell (InGaP/GaAs//InGaAs) with a simulated overall efficiency of 34%. The elimination of the graded buffer reduces fabrication cost while allowing for thicker base layers, increasing efficiency without increasing cost. A summary of the three considered cell structures and efficiencies are tabulated in Table 1.

Table 1. Summary of AM1.5G efficiencies of three triple-junction structures considered

	Theoretical η	**Experimental η**	**Simulated η**
InGaP/GaAs/Ge (LM)	39.61% [7]	32.3% [5]	25%
InGaP/GaAs/InGaAs (IMM)	42.01% [7]	33.8% [6]	33.5%
InGaP/GaAs//InGaAs	40.14% [8]	34% [8]	34%

Considering the comparable efficiencies between two and four terminal InGaP/GaAs/InGaAs structures, the doping levels, base thickness, and emitter thicknesses for the InGaP/GaAs dual junction and InGaAs single junction cells were optimized for efficiency under an AM1.5G spectrum with a triple-junction structure. This structure was determined to be the optimal combination of efficiency and cost.

II. Technical Background

The basic operation of a solar cell depends on the generation of charge carriers via the excitation of electrons to the conduction band by absorbing energy in the form of photons. The electrons and holes generated must then be separated and each charge carrier collected at opposite contacts on the solar cell. The movement of these carriers gives rise to a current and the separation yields a voltage across an attached load. A diagram of a basic pn junction is shown below in Figure 1. [9]

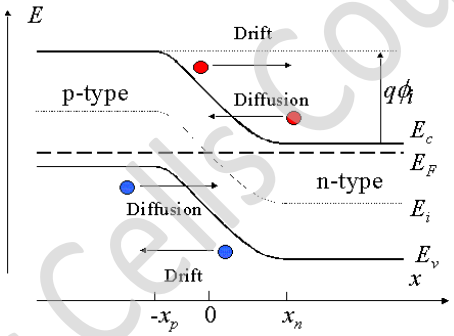

Figure 1. Illustration of pn junction band diagram with drift and diffusion currents labeled. [9]

The electrons, depicted in red, drift towards the right while the holes, depicted in blue, drift towards the left due to built-in electric field across the depletion region from $-x_p$ to x_n. The fundamental current voltage relationship used to model this behavior is known as the ideal diode equation and is shown in Equation 1. The incorporation of resistive and recombination effects can be modeled as a series of resistors and a double diode model, respectively. This modified diode equation is shown in Equation 2.

$$J(V) = J_{ph} - J_0\left[e^{\frac{qV}{kT}} - 1\right] \qquad \textbf{Eq. (1)}$$

$$J(V) = J_{ph} - J_{01}\left[e^{\frac{q(V+JR_s)}{kT}} - 1\right] - J_{02}\left[e^{\frac{q(V+JR_s)}{kT}} - 1\right] - \frac{V + JR_s}{R_{sh}} \qquad \textbf{Eq. (2)}$$

J_{ph} is the photocurrent density, whereas J_{01} and J_{02} are the dark current densities under ideality factors of n=1 and n=2, indicating radiative and nonradiative recombination, respectively. R_s represents the series resistance due to resistance through the semiconductor layers or between the semiconductor and metal contact. R_{sh} represents the shunt resistance due to alternative current paths such as material defects. The resulting JV curve in the dark and under illumination is illustrated in Figure 2a. The output power curve obtained by multiplying the current and voltage is shown in Figure 2b. [10] To obtain maximum efficiency, the solar cell should operate at the maximum power point (MPP).

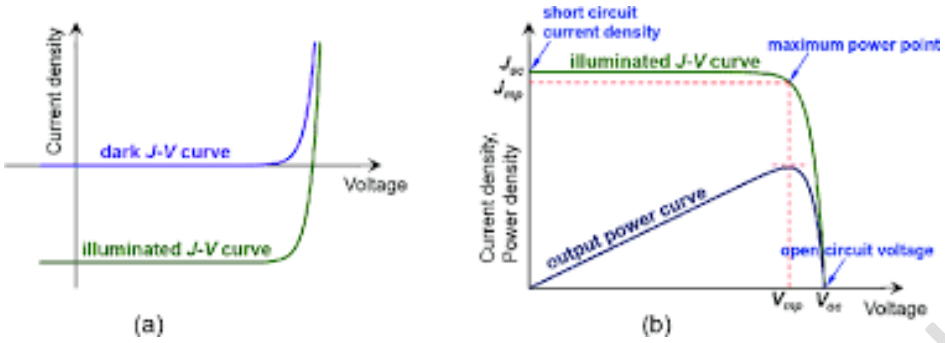

Figure 2. Illustration of JV curves (a) in the dark and under illumination and (b) the resulting power output [10]

Figures of merit such as fill factor (FF), open circuit voltage (V_{oc}) and short circuit current (J_{sc}) can easily be extracted from such JV curves. Additionally, the cell efficiency and external quantum efficiency (EQE) can be calculated in equations 4 and 5, respectively.

$$FF = \frac{P_{MPP}}{V_{oc}J_{sc}} \quad \textbf{Eq. (3)}$$

$$\eta = \frac{P_{MPP}}{P_{in}} \quad \textbf{Eq. (4)}$$

$$EQE(\lambda) = \frac{carriers\ collected}{photons\ incident} \quad \textbf{Eq. (5)}$$

Ideally, the efficiency and EQE should both be 100% across the entire wavelength range; however, surface and defect induced recombination gives rise to an EQE shape shown in Figure 3. [11]

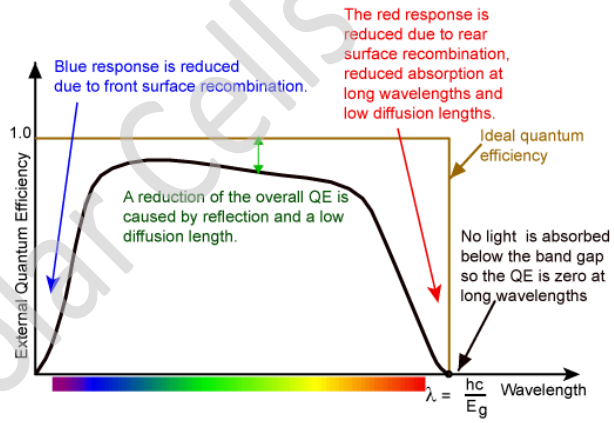

Figure 3. Realistic EQE curve with typical recombination pathways indicated. [11]

One method to improve the quantum efficiency at short wavelengths of light is the addition of a window layer. This large bandgap layer allows photons to enter the active region but prevents minority carriers from traveling to the front surface and recombining. To improve the QE at long wavelengths, the addition of a back surface field (BSF) is often used, as this prevents minority carriers from recombining at the back surface of the semiconductor via an energy barrier. Light with energy less than the bandgap is not absorbed, and light with energy much greater than the bandgap tends to lead to excess thermalization losses, restricting the output voltage. Thermalization occurs when electrons excited to above the conduction band minimum (CBM) relax down to the CBM, losing the difference in energy to heat. Thus, while smaller bandgap materials may have a higher current density due to the large amount of photons absorbed, larger bandgap material have a higher voltage due to the absorption of higher energy photons.

A basic single junction solar cell with the contacts, window, emitter, base, and BSF is shown in Figure 4 as an illustration of how a typical III-V cell looks. An anti-reflective coating is also added on top. [12]

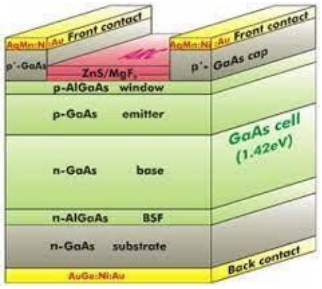

Figure 4. Illustration of a typical single junction solar cell. [12]

To harness the maximum fraction of the solar spectrum, multiple solar cells with different bandgaps may be utilized to capture different regions of the irradiation. Larger bandgap materials are placed above smaller bandgap semiconductors to allow the lower energy photons not absorbed through, where they get a second chance at absorption with the lower bandgap material. With electrically connected multi-junction structures, the addition of tunnel junctions (TJ) between individual cells is necessary to prevent parasitic reverse current from flowing due to the inverted n-p junction. These highly doped, large bandgap materials allow photons to pass through them while aligning the conduction and valence bands for charge carriers to tunnel from one cell to the next. Additionally, because each cell is essentially electrically connected in series to the others, each layer in a multi-junction solar cell should be current matched to the others. Whereas the output voltage is the addition of the output voltages of each cell, the layer with the smallest current output will throttle the current output of the entire device. There are three main fabrication methods for multi-junction solar cells: monolithically integrated cells, metamorphic cells, and mechanically stacked cells.

Monolithically integrated cells are the most limiting regarding which materials may be used in the solar cell stack due to the lattice matching requirement. Because each layer is successively grown on top of each other, each layer must be lattice matched to the layer it is grown on. Low but non-negligible lattice mismatch will impart strain on both layers, potentially altering the band structure and electron transport behavior. Conversely, threading dislocations will begin forming for larger lattice mismatch materials, which severely degrade the material quality and introduces recombination sites. Thus, the most common semiconductor stack used for monolithically integrated solar cells is InGaP/GaAs/Ge since these semiconductors are lattice matched to each other and their bandgaps absorb distinct but adjacent regions of the solar spectrum. Although their bandgaps are not perfectly matched to absorb the maximum fraction of the spectrum, the lattice matching condition precludes most other semiconductors from being used with monolithic multi-junction solar cells.

Metamorphic (MM) and inverted metamorphic (IMM) cells expand the list of possible materials with the addition of a graded buffer region, which gradually increases the lattice constant of a semiconductor until it is lattice matched to its neighbor. This is done by altering the composition of the ternary III-V compound in accordance with Vegard's law, shown in Equation 6.

$$a_{A_xB_{1-x}C} = xa_{AC} + (1-x)a_{BC} \qquad \textbf{Eq. (6)}$$

The lattice parameter of the ternary compound is $a_{A_xB_{1-x}C}$, whereas the lattice parameter of the binary AC compound is a_{AC} and a_{BC} for the binary BC compound. "x" is the mole fraction of element A in the ternary compound. These cells allow for material selection better suited for covering the entire solar spectrum. Under the InGaP/GaAs/Ge structure, the bottom Ge cell's bandgap is too small and encompasses portions of the solar spectrum with very small irradiation, leading to small output voltage. Without the lattice matching restriction, however, structures such as InGaP/GaAs/InGaAs can be created. $In_{0.3}Ga_{0.7}As$ has a bandgap of around 1.02eV, whereas Ge has a bandgap of around 0.67eV. This allows for higher voltage output from the structure while not sacrificing a significant portion of the solar spectrum. The efficiency of the InGaP/GaAs/InGaAs structure is shown in Figure 5. [13]

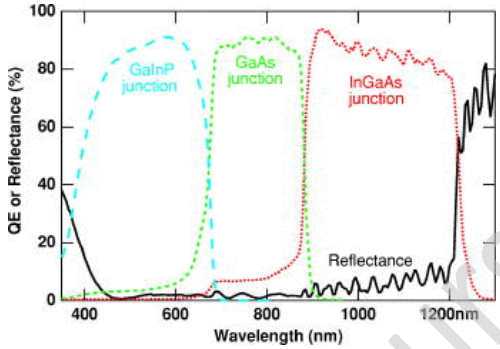

Figure 5. QE and reflectance of InGaP/GaAs/InGaAs solar cell [13]

InGaP/GaAs/InGaAs devices fabricated with inverted metamorphic method has demonstrated the 2010 world's highest efficiency for a triple-junction solar cell. [6] The lattice matched InGaP and GaAs cells are first monolithically grown. The buffer layer is then grown on top until the lattice constant is matched to InGaAs. The entire structure is then lifted off the GaAs substrate and inverted onto a separate handling substrate. While this method of growing triple-junction solar cells certainly can yield high efficiency cells, the addition of a buffer layer adds additional cost to the device and may not be ideal for this mobile device application which is the focus of this report.

The third alternative to electrically connecting each layer is to mechanically connect each cell with transparent, insulating layers. Each cell is then electrically contacted separately in series, so for a mechanically connected dual junction cell, there would be four terminals. This allows for the widest selection of semiconductor materials, as there are no lattice mismatch effects to consider.

A combination approaches 2 and 3 are used for this device design. The device detailed in the next section consists of a monolithic dual junction InGaP/GaAs cell mechanically connected to an $In_{0.3}Ga_{0.7}As$ single junction bottom layer. This combines the high efficiency seen with the IMM InGaP/GaAs/InGaAs structure with the cost effectiveness and fabrication ease of the mechanically stacked approach. Because the dual junction cell is the current limiting part of the design, the doping and base thicknesses for InGaP and GaAs were optimized to yield the highest current possible. Conversely, the doping and base thickness for the InGaAs cell was systematically varied and optimized for the highest voltage at the maximum power point. This combination of high current from the dual junction and high voltage from the single junction yields the highest overall efficiency once both cells are contacted.

III. Simulation Optimization and Results

To simulate the dual junction cell electrically and optically, technology computer aided design (TCAD) simulations were used with the Advanced Physical Models of Semiconductor Devices (APSYS) application in the Crosslight software. Crosslight was used due to its user-friendly interface and powerful

functionality in a wide range of applications. Basic carrier transport equations are integrated within the software and is based on 2D/3D finite element analysis to solve the semiconductor structure optically, electrically, and thermally. This software also has a wide range of III-V materials imbedded in its database. Any materials not preloaded into the database can be added by creating a spreadsheet of refractive index and extinction coefficient values.

The simulation process was split into two segments: optimizing the dual junction InGaP/GaAs cell and optimizing the InGaP cell. The dual junction structure yielding the highest J_{sc} was combined with the InGaAs structure that yielded the highest V_{oc}, giving the highest overall efficiency.

A. Optimization of InGaP/GaAs Dual Junction Cell

Because of the larger bandgap of InGaP and GaAs compared to InGaAs, this dual junction cell will be the current limiting portion of the triple-junction stack but yields higher voltage than the InGaAs cell. Thus, the doping level and GaAs base thickness were systematically varied and the combination yielding the highest current density was chosen as the final structure. A brief investigation into the doping level and base thickness of the InGaP cell was also done but the effect of varying these parameters was significantly smaller than that of the GaAs cell. For brevity of this report, these results are not included here. The final structure of this dual junction cell is shown in Figure 6.

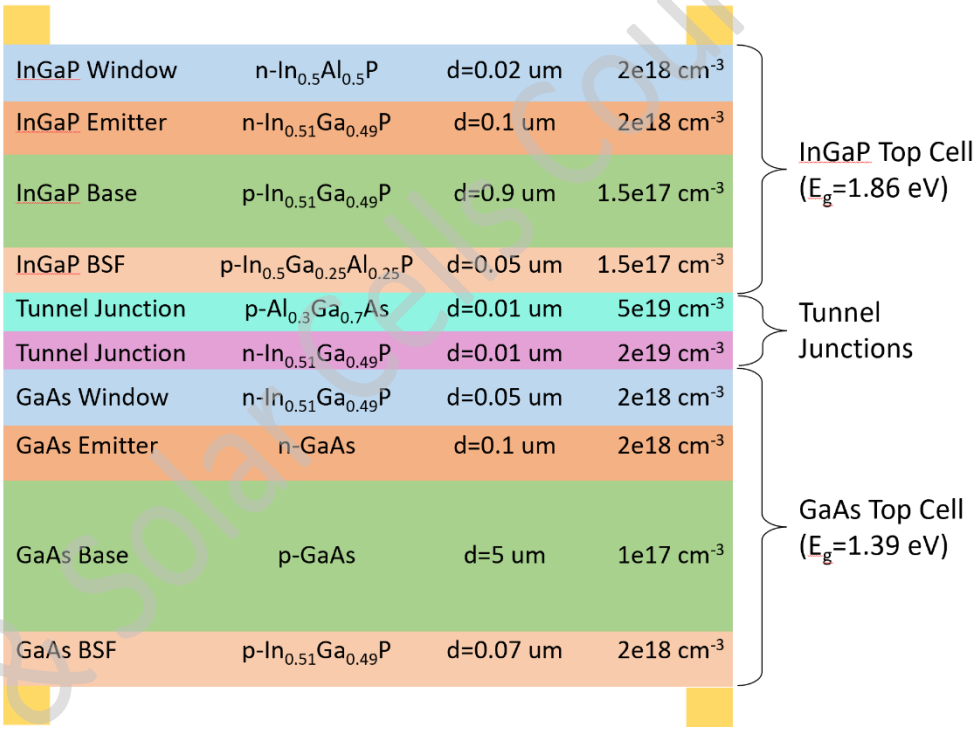

Figure 6. Device structure of dual junction InGaP/GaAs solar cell with layer functionality, composition, width, and doping level.

Because the InGaAs cell will be mechanically attached to this cell with an insulating layer, the bottom contact cannot block all the remaining light from entering the InGaAs cell; thus, during fabrication, they should be fabricated as small contacts like the top contacts. Using a typical deposition scheme, the contacts can be 100nm of Au on top of 10nm of Ti. Au is used for its superior conductivity and work function, as it would create an ohmic contact to the top and bottom of the stack, allowing current to freely flow between the two materials. Ti is used to promote adhesion of the gold to the semiconductor. The thicknesses are thick enough to collect the carriers while not being too thick to

contribute significant series resistance to the stack. Although the contacts were simply modeled as "ohmic" in Crosslight, contact material selection is important if these structures are to be fabricated.

With regards to altering the GaAs base thickness and doping, table 2 summarizes the variables altered and important figures of merit such as J_{MPP}, V_{MPP}, and efficiency for all combinations attempted.

Table 2. Summary of thickness and doping varied and figures of merit such as Jsc, Voc, and efficiency.

Thickness (um)	Doping (cm^{-3})	J_{MPP} (mA/cm^2)	V_{MPP} (V)	Efficiency (%)
4	8e16	11.89	2.293	27.15
4	1e17	11.93	2.283	27.23
4	2e17	11.89	2.283	27.16
4	3e17	11.87	2.283	27.11
4	4e17	11.85	2.283	27.04
4	5e17	11.87	2.271	26.97
2.5	1e17	11.68	2.283	26.66
2.75	1e17	11.75	2.283	26.82
3	1e17	11.81	2.283	26.97
3.5	1e17	11.90	2.283	27.17
4.5	1e17	11.96	2.283	27.31
5	1e17	12.17	2.248	27.35
8	1e17	12.28	2.236	27.47

The cell with the highest J_{sc} without sacrificing significant V_{oc} is highlighted. Although the combination with the base thickness of 8um yielded higher current, further increases in the base thickness past 5 um shows diminishing returns on the J_{sc}. Thus to save material and thus cost and to increase the V_{oc}, a base thickness of 5um and a doping of 1e17 cm^{-3}were chosen.

The band diagram of this structure is shown in Figure 7, whereas the relative energy density along the "y" direction is shown in Figure 8. Because the material and simulation parameters were constant in the "x" direction, the relative energy density is also constant in the "x" direction. Thus, only the 2D view is shown for viewing clarity.

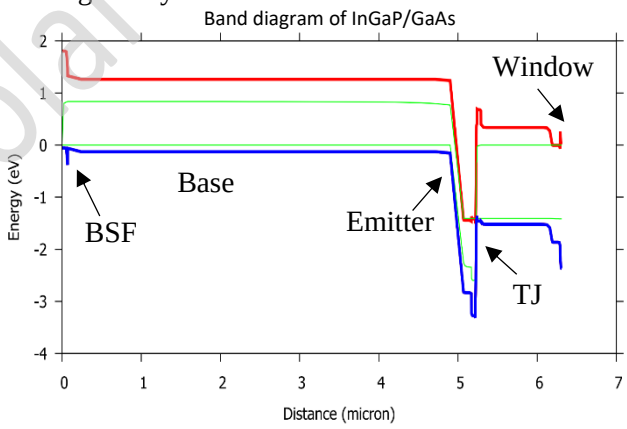

Figure 7. Band diagram of InGaP/GaAs dual junction cell under illumination with included features indicated.

As shown in the band diagram, the BSF prevents electrons from drifting to the back surface to recombine. TJ layers promote tunneling between GaAs and InGaP, and the window prevents holes from drifting to the front surface.

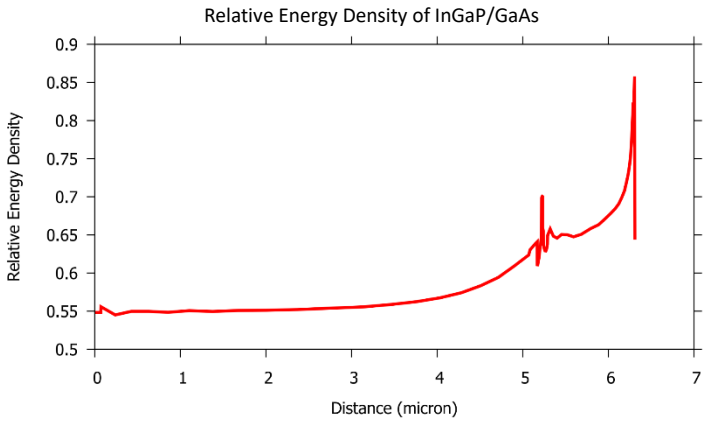

Figure 8. Relative energy density of dual junction InGaP/GaAs device.

B. Optimization of InGaAs Single Junction Cell

The current limiting portion of this triple-junction cell is the InGaP/GaAs dual junction cell. Thus, the single junction InGaAs cell was optimized for the highest possible operating voltage since the overall current density will be throttled to that of the dual junction cell. The InGaAs base thickness and doping were again systematically varied until the combination with the highest V_{oc} is reached. A summary of figures of merit are shown in Table 3.

Table 3. Summary of InGaAs parameters varied and corresponding figures of merit.

Thickness (um)	**Doping (cm^{-3})**	**J_{MPP} (mA/cm^2)**	**V_{MPP} (V)**	**Efficiency (%)**
4	1e17	40.41	0.481	19.43
4	5e17	39.80	0.539	21.47
4	7e17	40.90	0.539	22.06
4	1e18	41.72	0.539	22.50
3.5	5e17	41.49	0.516	21.41
3.5	7e17	40.17	0.539	21.66
2.5	1e18	40.15	0.539	21.66
1.2	1e18	39.04	0.516	20.14
1.5	1e18	41.50	0.493	20.44
1.75	1e18	38.48	0.539	20.75
1.6	1e18	40.73	0.504	20.54
1.7	1e18	39.18	0.528	20.67

The highlighted cell was chosen as the combination of base thickness and doping level due to the high operating voltage. While there were several combinations that yielded this operating voltage, this combination was obtained for the thinnest base layer, saving material and cost. As the thickness of the base decreases, the current density also decreases because fewer carriers are being absorbed in the active region before the light transmits through the device.

As the base doping increases, more charge carriers are injected into the solar cell, increasing the width of the depletion region. This is especially important for semiconductors with carrier lifetimes smaller than that of GaAs since a wider depletion region means more carriers can make it to the depletion region to be separated and contribute to the output current. Thus, increasing the doping within realistic values obtainable through MOCVD or MBE should increase the efficiency of the cell, which is indeed what is observed in Table 3. The resultant structure chosen is shown in Figure 9.

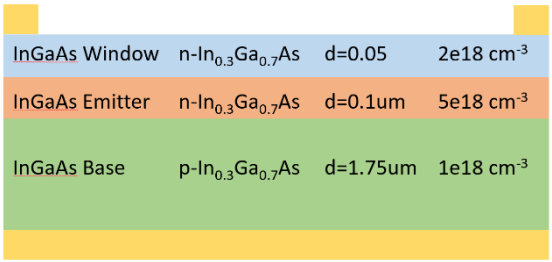

Figure 9. Optimized structure of single junction InGaAs cell.

Because there is no longer a cell that needs to be below this cell, the entire back of the single junction cell can be covered in metal, decreasing the sheet resistance, and increasing the carrier collection efficiency, as the carriers do not have to travel to the small contacts on either side to contribute to current. The resulting band diagram is shown in Figure 10 and the energy density is shown in Figure 11.

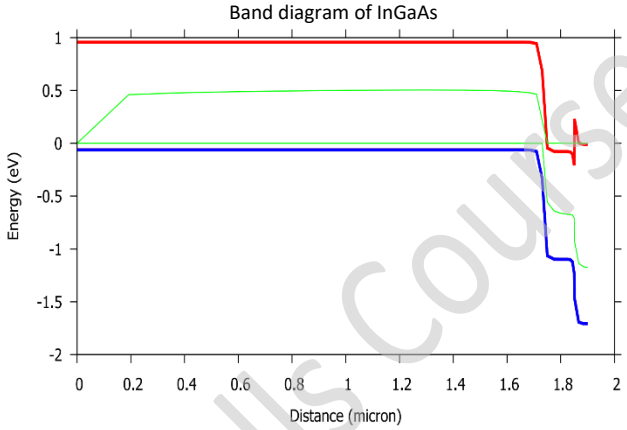

Figure 10. Band diagram of single junction InGaAs solar cell under illumination.

Similar features as the dual junction cell are present in this cell apart from the BSF layer. Because the entire backside is coated in metal, the concern for back surface recombination is lessened compared to that in the dual junction case. The Ti layer between the InGaAs and gold also helps passivate the surface and decrease the number of possible recombination sites.

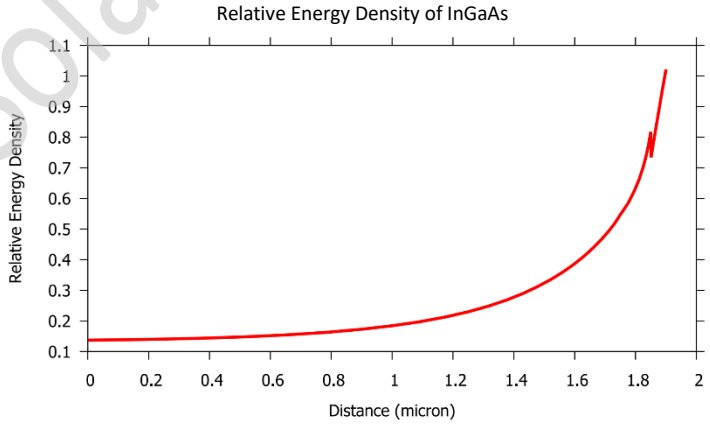

Figure 11. Relative energy density of InGaAs single junction cell

These optimal base dopings and thicknesses were then put together in the InGaP/GaAs//InGaAs structure. The stack was not simulated in Crosslight; rather, the operating current was taken from the dual junction cell and the operating voltage was calculated by adding the V_{MPP} from both cells.

C. Optimization of InGaP/GaAs//InGaAs Triple Junction Cell

As previously mentioned, the dual junction structure with the highest operating current density and the single junction structure with the highest operating voltage were analyzed together as if they were mechanically attached together in series. During fabrication and testing, there would be four terminals to this device attached in series. This allows for the operating voltage to be high enough to charge an iPad. The resulting JV curves and power output curves for the dual and single junction cells are shown in Figures 12a and b, respectively.

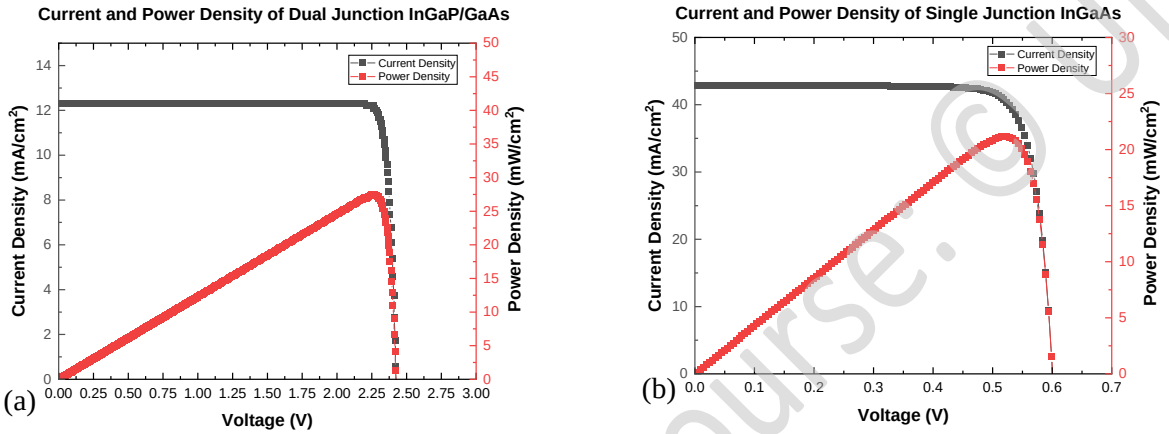

Figure 12. Current and power density plots of the (a) dual junction InGaP/GaAs cell and (b) the single junction InGaAs cell.

Looking at the horizontal and vertical scaling of these plots, the dual junction is the current limiting factor here. Thus, the J_{MPP} of the entire stack was taken to be 12.17 mA/cm^2 and the V_{MPP} to be 2.787V. This yields an overall efficiency of about 34%, which is on par with experimental results. The JV curves of both the single and dual junction cells are coplotted in Figure 13 for ease of visual comparison.

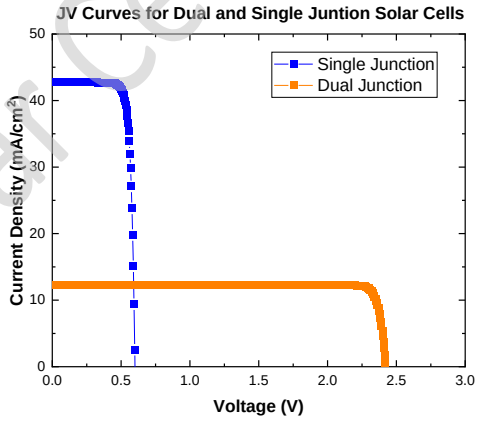

Figure 13. JV curves of single and dual junction cells coplotted.

To put these results into the framework of an iPad, the standard 12W charger which comes with the iPad 7 models supports a voltage of 5.2V and 2.4A. [14] Given the surface area of the back of an iPad 7th generation is 250.6mm x 174.1 mm, the current output of one solar cell the size of the iPad would be 5.3A and the voltage output would be 2.78V. [15] Halving the size of the solar cell and connecting two in series would lead to a current output of 2.65 A and a voltage output of 5.57V, leading to an output power of 14.8W. This is slightly higher than the output power of the Apple iPad charger, meaning leaving the iPad face down in the sun for a few minutes would be enough to power up the device until a cord could be found. In the context of an iPhone 13, the output current and voltage of an array the size of the iPhone

would be 1.276 A and 2.787 V, respectively, which corresponds to an output power of 3.56W. [16] Compared to the standard 5W charger which comes in the iPhone box, the power output is too low to fast charge the device. However, it is still enough power to charge the device fast enough to power it on and provide enough electricity for a few phone calls in an emergency.

D. Financial Feasibility Study

While it is difficult to estimate the cost of producing such an array, NREL has released a techno-economic analysis of the cost of III-V cells. In the triple junction, lattice matched case of InGaP/GaAs/Ge they use, the estimated cost of such a cell at a 200kW/yr production level is \$70/W_{DC} with all manufacturing costs included. [17] For this array, this means a cost of \$1031 for the iPad size and \$250 for the iPhone size. While the price for the iPhone case may be in reach for some upper middle-class people, the cost for the iPad version is likely to restrict the sale of such arrays to the wealthy upper class.

Because much of the manufacturing cost is related to the upstart cost of purchasing and optimizing an MOCVD system, the more arrays produced, the cheaper the technology will be. Thus, to fully take advantage of this proposed device, an established mobile device case company such as Otterbox or Spec will need to invest in an MOCVD system. While the technology has been simulated here, there are still several outstanding hurdles to be crossed before the widespread implementation of such a device.

IV. Conclusions and Summary

As the world becomes increasingly dependent on mobile devices such as iPhone and iPads for everything from entertainment to contacting emergency services, the integration of renewable energy is increasingly important from an environmental and an economic standpoint. While the amount of power consumed for mobile devices is near negligible compared to automobiles and factories, the integration of an instantaneous power source to a mobile device has many applications, especially during emergencies. Thus, the efficiency of a triple-junction III-V solar cell was optimized in this report based on base thicknesses and doping concentrations. Because the dual and single junction cells are connected in series, material parameters for the dual junction cell were varied to yield the highest output current possible while the single junction cell was optimized to yield the highest output voltage. Upon connecting these two cells mechanically with four terminals, the overall cell yielded a current density at the maximum power point (MPP) of 121.67 A/m^2 and a voltage at the MPP of 2.787V. This is enough power to fast charge an iPad when the entire back of the iPad is covered in solar cells and enough to standard charge an iPhone.

Although the technological feasibility has been proven in this report, fabricating high quality materials and interfaces may further hamper the efficiency of this cell, decreasing the potential power output. Additionally, the high cost especially for the iPad precludes most Americans from purchasing such an array. Widespread investment in MOCVD technology would certainly bring the cost down, but the mobile device market is not yet ready for such a large upfront investment.

Avenues of future simulation work include investigating more material variables such as carrier lifetime, emitter doping and thickness, and the addition of an anti-reflective coating on the top of the cell. The further optimization of this device would yield higher efficiency and a smaller amount of material required to produce the same output power. The natural next step towards realizing this technology is the fabrication with MOCVD. There are additional optimization avenues required to obtain the high crystal and interface quality required for the fabricated device to perform as well as the simulated device. Once proven in the lab setting, the widespread implementation of such a device is required to drive the price down. The simulations done in this report provide the technological groundwork required for the realization of such a device.

References

[1] Solar Technologies Office, "Crystalline Silicon Photovoltaics Research," Office of Energy Efficiency and Renewable Energy, [Online]. Available: https://www.energy.gov/eere/solar/crystalline-silicon-photovoltaics-research#:~:text=Crystalline%20silicon%20PV%20cells%20have,22%25%20under%20standard%20test%20conditions.. [Accessed 18 April 2022].

[2] Solar Energy Technologies Office, "Multijunction III-V Photovoltaics Research," Office of Energy Efficiency and Renewable Energy, [Online]. Available: https://www.energy.gov/eere/solar/multijunction-iii-v-photovoltaics-research#:~:text=Three%2Djunction%20devices%20using%20III,other%20materials%20are%20being%20investigated.. [Accessed 18 April 2022].

[3] N. W. Stauffer, "Transparent Solar Cells," MITEI, 20 June 2013. [Online]. Available: https://energy.mit.edu/news/transparent-solar-cells/. [Accessed 18 April 2022].

[4] A. H. Munshi, J. M. Kephart, A. Abbas, T. M. Shimpi, K. L. Barth, J. M. Walls and W. S. Sampath, "Polycrystalline CdTe photovoltaics with efficiency over 18% through improved absorber passivation and current collection," *Sol. Energy Mater. and Sol. Cells*, vol. 176, pp. 9-18, 2018.

[5] D. Aiken, "InGaP/GaAs/Ge multi-junction solar cell efficiency improvements using epitaxial germanium," *Conference Record of the Twenty-Eighth IEEE Photovoltaic Specialists Conference - 2000*, vol. Cat. No. 00CH37036, pp. 994-997, 2000.

[6] T. Takamoto, T. Agui, A. Yoshida, K. Nakaido, H. Juso, K. Sasaki, K. Nakamora, H. Yamaguchi, T. Kodama, H. Washio, M. Imaizumi and M. Takahashi, "World's Highest Efficiency Triple-Junction Solar Cells Fabricated by Inverted Layers Transfer Process," *2010 35th IEEE Photovoltaic Specialists Conference*, pp. 000412-000417, 2010.

[7] O. Saif, "On the optimization of InGaP/GaAs/InGaAs triplejunction solar cell," *8 IOP Conf. Ser.: Mater. Sci. Eng. 4*, 2018.

[8] T. Takamoto, E. Ikeda, T. Agui, H. Kurita, T. Tanabe, S. Tanaka and H. Matsubara, "InGaP/GaAs and InGaAs mechanically-stacked triple-junction solar cells," *Conference Record of the Twenty Sixth IEEE Photovoltaic Specialists Conference*, pp. 1031-1034, 1997.

[9] Stack Exchange, October 2016. [Online]. Available: https://physics.stackexchange.com/questions/287272/the-band-diagram-of-a-p-n-and-metal-semiconductor-junctions/287282#287282. [Accessed 18 April 2022].

[10] Y. Tao, "Screen-Printed Front Junction n-Type Silicon Solar Cells," *Printed Electronics - Current Trends and Applications*, pp. 47-73, 2016.

[11] C. Honsberg and S. Bowden, "Quantum Efficiency," PV Education, [Online]. Available: https://www.pveducation.org/pvcdrom/solar-cell-operation/quantum-efficiency. [Accessed 18 April 2022].

[12] Photovoltaics Lab IOFFE, "Solar Cells," PV Lab, [Online]. Available: http://pvlab.ioffe.ru/about/solar_cells.html. [Accessed 18 April 2022].

[13] J. Geisz, S. Kurtz and M. Wanlass, "High-efficiency GaInP/GaAs/InGaAs triple-junction solar cells grown inverted with a metamorphic bottom junction," *Appl. Phys. Lett.*, vol. 91, no. 023502, 2007.

[14] Apple, "About Apple USB Power Adapters," Apple, [Online]. Available: https://support.apple.com/en-us/HT210133. [Accessed 19 April 2022].

[15] Apple, "iPad Tech Specs," Apple, [Online]. Available: https://www.apple.com/ipad-10.2/specs/. [Accessed 19 April 2022].

[16] Apple, "iPhone 13 Tech Specs," Apple, [Online]. Available: https://www.apple.com/iphone-13/specs/. [Accessed 19 April 2022].

[17] K. A. Horowitz, T. W. Remo, Brittany Smith, and A. J. Ptak, "A Techno-Economic Analysis and Cost Reduction Roadmap for III-V Solar Cells", NREL, Golden, Colorado, rep., 2018.